



An exact analysis of the temperature control of optical waveguides

Frank Payne¹ · Zipei Song² · Mohan Wang² · Julian A. J. Fells²

Received: 28 October 2024 / Accepted: 28 January 2025 / Published online: 11 March 2025
© The Author(s) 2025

Abstract

In this paper we present an exact analysis of the variation with temperature of the effective index of an arbitrary optical waveguide. Our results allow the design of temperature compensated devices using only a single parameter calculated at one temperature avoiding the need to perform an analysis over a range of temperatures. We derive expressions for both weakly and strongly guiding waveguides. We derive a complete analytical solution for the design of micro channel fibers where the micro channels are filled with a temperature compensating material whose refractive index equals that of the fiber cladding at a specified reference temperature. We also analyse the more general case including the effects of thermal expansion. We illustrate our analysis with the application to athermal fiber Bragg gratings and arrayed waveguide grating filters.

Keywords Athermal waveguide · Temperature compensated waveguide · Optical fiber · Fiber Bragg grating · Arrayed waveguide grating · Micro-channel fiber

1 Introduction

The propagation of light through an optical waveguide is affected by changes of temperature in two important ways: (i) thermal changes in the refractive indices of the waveguide materials, and (ii) thermal expansion of the waveguide or the substrate on which the waveguide is grown. The former results in a change with temperature of the effective index

Zipei Song, Mohan Wang and Julian A. J. Fells have contributed equally to this work.

✉ Frank Payne
frank.payne@lincoln.ox.ac.uk

Zipei Song
zipei.song@eng.ox.ac.uk

Mohan Wang
mohan.wang@eng.ox.ac.uk

Julian A. J. Fells
julian.fells@eng.ox.ac.uk

¹ Lincoln College, University of Oxford, Turl Street, Oxford OX1 3DR, UK

² Department of Engineering Science, University of Oxford, Parks Road, Oxford OX1 3PJ, UK

n_{eff} of the waveguide mode, and the latter causes a change of phase along the waveguide because of changes of the waveguide dimensions. Both effects usually occur together and have an impact on the performance of a wide range of waveguide devices. For example, fiber Bragg gratings find many applications as sensors and optical filters (Kersey et al. 1997), and arrayed waveguide gratings (AWGs) have applications as wavelength division multiplexers and demultiplexers, as well as wavelength routers (Leijtens et al. 2006). In the case of a fiber Bragg grating, a change in temperature will cause a shift in the Bragg wavelength and impair the sensor response. In the case of an AWG, a change in temperature will cause a shift in the filter's center wavelength and free spectral range, as well as misalignment with the ITU grid (Leijtens et al. 2006; Okamoto 2000). Other examples include systems where variations with temperature of the propagation time through an optical fiber adversely affects performance. Examples include the synchronization of optical data signals and clocks. A review of these and other applications can be found in Fokoua et al. (2017).

Most waveguide cores are made from materials with a positive thermo-optic coefficient dn/dT , and a common way to mitigate the effects of temperature change is by incorporating materials with a negative thermo-optic coefficient into the waveguide design. Athermal AWGs made using silica-on-silicon technology (Himeno et al. 1998; Ou 2003) have been demonstrated. In Inoue et al. (1997); Kamei et al. (2009) a silicone wedge is inserted into a groove cut into the array of silica waveguides, and in Li et al. (2007) a polymer cladding with negative dn/dT is used. A similar approach has been applied to AWGs made with silicon-on-insulator technology (Jalali et al. 1998; Ye et al. 2008; Wang et al. 2009, 2012), and all-polymer AWGs (Keil et al. 2001).

The athermal design of fiber Bragg gratings has been demonstrated by creating micro-channels around the fiber core which are filled with a liquid with a negative thermo-optic coefficient (Man et al. 2019; Mothe et al. 2008; Huy et al. 2008; Song et al. 2025).

The published literature describes a variety of methods for reducing the effects of temperature on waveguide devices. A common feature is a theoretical model for the variation of the modal effective index with temperature. Several different models have been reported. In some cases the temperature variation of n_{eff} is related to the refractive indices of the waveguide core and cladding, weighted in proportion to the modal power carried by each. In others, dn_{eff}/dT is related to the rate of change of core and cladding indices, also weighted by the modal power fraction carried by each. There is no detailed derivation of any of these approximate results. It is the purpose of this paper to present an exact and rigorous analysis of the variation of n_{eff} with temperature, and to derive exact equations for dn_{eff}/dT that allows the design of a wide range of waveguide devices without the need for device modelling over a range of temperatures. Our analysis is valid for weakly guiding waveguides where the modes are described by the scalar wave equation. This is not a strong restriction as many waveguides are weakly guiding. We also derive the corresponding result for waveguides with large refractive index differences and which must be described by full vector modes, including birefringent waveguides.

In this paper we distinguish between temperature compensated waveguides and athermal waveguides. The former refers to waveguides in which only the temperature variation of the effective index is minimized, and the latter refers to waveguide devices where the effects of both thermal expansion and changes in the effective index are compensated.

This paper has eight sections. In Sect. 2 we discuss the temperature dependence of a step index optical fiber for which a direct calculation of dn_{eff}/dT is possible from first principles. We show how this result can be used to design and model a temperature compensated fiber. Section 3 derives an exact expression for dn_{eff}/dT valid for an arbitrary weakly guiding

waveguide structure and which relates dn_{eff}/dT to the modal power fractions in each waveguide region. The case where the temperature compensating regions have a refractive index equal to that of the fiber cladding at a particular reference temperature is analysed in Sect. 4. We consider fibers with microchannels consisting of either an annulus sector shape or side hole shape. For these cases the modal overlap fractions can be calculated exactly and it is possible to produce exact analytical results for temperature compensated designs with minimal computation. In Sect. 5 we discuss the more general situation where the refractive index of the compensating regions differs from that of the cladding. In Sects. 2, 4, and 5 we discuss practical ways of fabricating the waveguides analyzed, and we give estimates of the waveguide losses.

An athermal design must include the effects of thermal expansion, and we discuss this in detail in Sect. 6. For waveguides with large refractive index differences the weakly guiding scalar analysis is not valid and a full vector treatment is necessary. This is set out in detail in Sect. 7.

In Sect. 8 we compare our approach, which requires the calculation of only one parameter at one temperature, to that of others where the waveguide response must be computed over a range of temperatures. Finally, in Sect. 8 we present our conclusions.

2 Thermal analysis of the step index optical fiber

It is instructive to consider the temperature dependence of a step index optical fiber. The step index fiber is one of only a few examples where a direct calculation is possible of the temperature variation dn_{eff}/dT of the guided mode effective index.

We consider a weakly guiding optical fiber with core radius a , and refractive index n_1 , surrounded by an infinite cladding of refractive index n_2 . The fundamental LP_{01} mode is described by the scalar wave equation. The mode parameters u , w and V are defined by Okamoto (2000); Snyder and Love (1984); Adams (1981):

$$u = a\sqrt{n_1^2k^2 - \beta^2} ; w = a\sqrt{\beta^2 - n_2^2k^2} \tag{1}$$

$$V = ak\sqrt{n_1^2 - n_2^2} = \sqrt{u^2 + w^2} \tag{2}$$

The propagation constant is β and k is the free space wave number. The LP_{01} modal field is given by:

$$\psi = \begin{cases} AJ_0\left(\frac{ur}{a}\right) & \text{for } r \leq a, \\ A\frac{J_0(u)}{K_0(w)} \cdot K_0\left(\frac{wr}{a}\right) & \text{for } r > a \end{cases} \tag{3}$$

where J is a Bessel function of the first kind, and K is a modified Bessel function of the first kind (Abramowitz and Stegun 2013; Gradshteĭn and Ryzhik 1980). The modal field is normalised so that:

$$\int_0^\infty \int_0^{2\pi} \psi^2 r dr d\theta = 1 \tag{4}$$

The normalisation constant A is given by:

$$A = \frac{w}{aVJ_1(u)\sqrt{\pi}} \tag{5}$$

In deriving Eq. (5) we have made use of the eigenvalue equation that determines the propagation constant:

$$\frac{J_0(u)}{uJ_1(u)} = \frac{K_0(w)}{wK_1(w)} \tag{6}$$

Details of the derivation of Eqs. (1) to (6) can be found in Okamoto (2000); Snyder and Love (1984); Adams (1981). It is straightforward to show that the fractions of modal power in the core and cladding are given by:

$$\Gamma_1 = \int_0^a \int_0^{2\pi} \psi^2 r dr d\theta = 1 - \frac{u^2}{V^2} \cdot \left(1 - \frac{K_0^2(w)}{K_1^2(w)} \right) \tag{7}$$

$$\Gamma_2 = \int_a^\infty \int_0^{2\pi} \psi^2 r dr d\theta = \frac{u^2}{V^2} \cdot \left(1 - \frac{K_0^2(w)}{K_1^2(w)} \right) \tag{8}$$

The effective index n_{eff} is defined by $n_{\text{eff}} = \beta/k$. From Eq. (6), u is a function only of V , and from Eqs. (1) and (2) the effective index can be written as:

$$n_{\text{eff}}^2 = n_1^2 - (n_1^2 - n_2^2)f(V) \tag{9}$$

where $f(V) = u^2/V^2$. Differentiating Eq. (9) we obtain:

$$\frac{dn_{\text{eff}}^2}{dT} = \frac{dn_1^2}{dT}(1 - f(V)) + \frac{dn_2^2}{dT}f(V) - (n_1^2 - n_2^2)\frac{df}{dV} \cdot \frac{dV}{dT} \tag{10}$$

From the definition of V in Eq. (2) we find dV/dT is given by:

$$\frac{dV}{dT} = \frac{V}{2(n_1^2 - n_2^2)} \cdot \left(\frac{dn_1^2}{dT} - \frac{dn_2^2}{dT} \right) \tag{11}$$

and df/dV is given by:

$$\frac{df}{dV} = \frac{2u}{V^2} \left(\frac{du}{dV} - \frac{u}{V} \right) \tag{12}$$

Equation (12) includes du/dV which can be shown to be (Okamoto 2000):

$$\frac{du}{dV} = \frac{u}{V} \cdot \left[1 - \frac{K_0^2(w)}{K_1^2(w)} \right] \tag{13}$$

Combining Eqs. (10) to (13) gives the following result:

$$\frac{dn_{\text{eff}}^2}{dT} = \frac{dn_1^2}{dT} \cdot \left[1 - \frac{u^2}{V^2} \left(1 - \frac{K_0^2(w)}{K_1^2(w)} \right) \right] + \frac{dn_2^2}{dT} \cdot \left[\frac{u^2}{V^2} \left(1 - \frac{K_0^2(w)}{K_1^2(w)} \right) \right] \quad (14)$$

The effects of transverse and longitudinal thermal expansion have not been included in the derivation of Eq. (14). We consider these in Section 6. From Eqs. (7) and (8) we recognise the expressions in square brackets on the right hand side of Eq. (14) as Γ_1 and Γ_2 , the fractions of modal power in the core and cladding, so that Eq. (14) can be written more simply as:

$$\frac{dn_{\text{eff}}^2}{dT} = \Gamma_1 \frac{dn_1^2}{dT} + \Gamma_2 \frac{dn_2^2}{dT} \quad (15)$$

Equation (15) shows that the temperature dependence of n_{eff}^2 is given by the temperature dependence of n_1^2 and n_2^2 weighted by the fractions of modal power they each carry. Since $\Gamma_1 + \Gamma_2 = 1$ we can rewrite Eq. (15) in the following form:

$$\frac{dn_{\text{eff}}^2}{dT} = (1 - \Gamma_2) \frac{dn_1^2}{dT} + \Gamma_2 \frac{dn_2^2}{dT} \quad (16)$$

From Eq. (16) the condition for $dn_{\text{eff}}/dT = 0$ is given by:

$$\Gamma_2 = \frac{n_1 \frac{dn_1}{dT}}{n_1 \frac{dn_1}{dT} - n_2 \frac{dn_2}{dT}} \quad (17)$$

Equation (17) allows us to calculate the fraction of power in the fiber cladding that minimises the temperature variation of the waveguide mode's effective index. We discuss this in more detail in the next section.

2.1 Design of a temperature compensated step index fiber

We illustrate the theory developed in Sect. 2 with the design of a temperature compensated step index fibre which has $dn_{\text{eff}}/dT = 0$ at a reference temperature T_0 . We assume a core refractive index $n_1 = 1.451$, and $dn_1/dT = 8.45 \times 10^{-6}/^\circ\text{C}$ at $T_0 = 25^\circ\text{C}$, which corresponds to fused silica (Leviton and Frey 2006). We examine the design for a cladding refractive index $n_2 = 1.434$ with a temperature dependence $dn_2/dT = -394 \times 10^{-6}/^\circ\text{C}$, which is available from the range of siloxane and aliphatic / alicyclic hydrocarbon based refractive index liquids manufactured by Cargille Laboratories, data sheet: Refractive-Index-Liquid-Series-AA-n-1.4440-at-589.3-nm-and-25°C (Cargille). A wavelength of 1550 nm is assumed. From Eq. (17) the required value of Γ_2 is 0.0212. The modal power fraction Γ_2 was calculated as a function of the core radius a , using Eqs. (6) and (8). The results are shown in Fig. 1. The dashed line (b) drawn at $\Gamma_2 = 0.0212$ shows the core radius for which a design can exist. From Fig. 1 the required core radius for a temperature compensated design is 6.24 μm .

We define the fractional change in the effective index Δn_{eff} by:

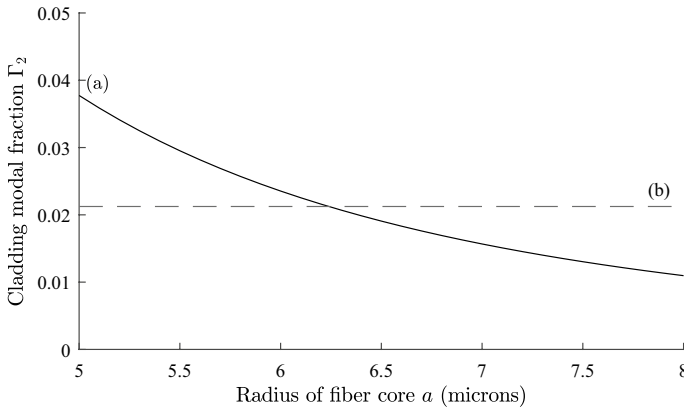


Fig. 1 Plot of Γ_2 , fraction of power in cladding as a function of core radius a for a step index fiber with cladding refractive index 1.434 curve **a**. The horizontal line **d** indicates where $\Gamma_2 = 0.0212$

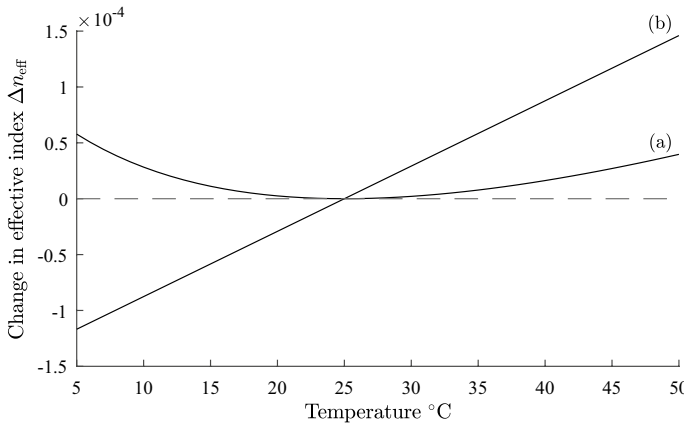


Fig. 2 Plot of fractional change in effective index Δn_{eff} against temperature for a step index fibre. Curve **a** is for a temperature compensated design with parameters defined in Sect. 2.1, and curve **b** is for an uncompensated fiber where core and cladding both vary as $dn/dT = 8.45 \times 10^{-6}/^\circ\text{C}$

$$\Delta n_{\text{eff}} = \frac{n_{\text{eff}}(T) - n_{\text{eff}}(T_0)}{n_{\text{eff}}(T_0)} \tag{18}$$

In Fig. 2, curve (a), Δn_{eff} is shown as a function of temperature T for a step index fiber with a core radius of $6.24 \mu\text{m}$ and with the other parameters given above. Also, shown for comparison in curve (b), is the variation of Δn_{eff} with temperature for an uncompensated fiber where both core and cladding indices vary as $dn/dT = 8.45 \times 10^{-6}/^\circ\text{C}$. For the temperature compensated design the maximum variation of Δn_{eff} is about 5×10^{-5} , whereas for the uncompensated fiber it is 26.4×10^{-5} . The predicted zero of dn_{eff}/dT at 25°C is evident in Fig. 2. Using Eq. (17) the single plot of Γ_2 in Fig. 1 gives the value of the fiber core for which a temperature compensated design can exist for the parameters specified and without the need to perform repeated calculations of Δn_{eff} as a function of temperature.

The simplicity of the step index fiber design raises the question of practical methods of fabrication. There are two widely used techniques described in the literature. The first is based on chemical etching (Ascorbe et al. 2016; Meunier et al. 2023; Zaca-Morán et al. 2018; Kim et al. 2012). In this method the outer protective acrylate coating of the fiber is removed over a length from a few mm to a few cms. The outer cladding of the fiber is then gradually removed by etching in a solution of hydrofluoric acid (HF). By varying the concentration of HF, and the etching time, it is possible to completely remove the fiber cladding and expose the fiber core which can then be immersed in the temperature controlling refractive index liquid. This method has been used to demonstrate a temperature compensated fiber Bragg grating (Kim et al. 2012).

The second method of fabrication is based on tapering the fiber by the heat and draw method (Hale et al. 1996; Hale and Payne 1994; Pendock et al. 1993; Henry and Payne 1995; Gao et al. 2012). In this method the outer protective acrylate fiber coating is removed and a section of bare fiber is heated in an oxy-butane or oxy-propane flame. As the fiber melts it is extended so that the original cladding is reduced to a few microns and the original core is reduced to fractions of a micron. By careful control an adiabatic taper results so that the waveguide mode gradually evolves from one guided by the original fiber core to one guided by the reduced diameter cladding which allows interaction with the surrounding temperature controlling liquid. A temperature compensated fiber Bragg grating has also been demonstrated using this method (Gao et al. 2012).

The optical loss of the temperature compensated step index fiber can be estimated from the loss of the refractive index liquid. For the Cargille Laboratories liquid cited above the optical transmission is quoted as 76% over one cm, corresponding to an optical loss of $L = 1.2\text{dB/cm}$ (Cargille). The fraction of optical power propagating in the liquid is Γ_2 so that the combined loss is given by $\Gamma_2 L$ (Adams 1981). For $\Gamma_2 = 0.0212$ this corresponds to a device loss of 0.025dB/cm .

3 Thermal analysis of a general optical waveguide

In this section we derive an exact expression for the rate of change with temperature of the effective index of a weakly guiding optical waveguide shown in cross section in Fig. 3.

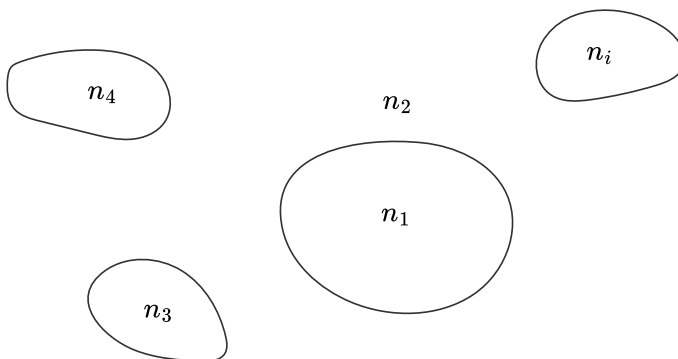


Fig. 3 A general optical waveguide with core of refractive index n_1 , infinite cladding of index n_2 and temperature controlling regions of index n_3, n_4, \dots, n_i

The core is of arbitrary cross section with refractive index n_1 and the infinite cladding has index n_2 . Within the cladding are temperature controlling regions of arbitrary shape, parallel to the waveguide axis. For completeness, we consider the general case where the refractive indices n_3, n_4, \dots, n_i can take arbitrary values. In the weakly guiding approximation, and at temperature T , the modal wave function $\psi = \psi(T)$ satisfies the scalar wave equation (Snyder and Love 1984):

$$\nabla_t^2 \psi + k^2 n^2 \psi = \beta^2 \psi \tag{19}$$

where

$$\nabla_t^2 = \frac{\partial}{\partial x^2} + \frac{\partial}{\partial y^2} \tag{20}$$

The refractive index varies with temperature as $n = n(T)$, the free space wave number is k , and the propagation constant is $\beta = \beta(T)$. At temperature $\bar{T} = T + \delta T$ the wave equation becomes

$$\nabla_t^2 \bar{\psi} + k^2 \bar{n}^2 \bar{\psi} = \bar{\beta}^2 \bar{\psi} \tag{21}$$

where $\bar{\psi} = \psi(\bar{T})$, $\bar{n} = n(\bar{T})$, and $\bar{\beta} = \beta(\bar{T})$. We now multiply Eq. (19) by $\bar{\psi}$ and Eq. (21) by ψ , subtract and integrate over all space:

$$(\beta^2 - \bar{\beta}^2) \int \bar{\psi} \psi \, dA = k^2 \int (n^2 - \bar{n}^2) \bar{\psi} \psi \, dA + \int (\bar{\psi} \nabla_t^2 \psi - \psi \nabla_t^2 \bar{\psi}) \, dA \tag{22}$$

The last integral in Eq. (22) can be rewritten using Green’s second identity (Arfken et al. 2013):

$$\begin{aligned} \int (\bar{\psi} \nabla_t^2 \psi - \psi \nabla_t^2 \bar{\psi}) \, dA &= \int \nabla_t \cdot (\bar{\psi} \nabla_t \psi - \psi \nabla_t \bar{\psi}) \, dA \\ &= \oint (\bar{\psi} \nabla_t \psi - \psi \nabla_t \bar{\psi}) \cdot \hat{\mathbf{n}} \, dl \end{aligned} \tag{23}$$

In Eq. (23), dl denotes a line integral with outward normal $\hat{\mathbf{n}}$ around the boundary of integration which is assumed to extend to infinity where ψ and $\nabla_t \psi$ vanish. The line integral in Eq. (23) is then zero and Eq. (22) reduces to

$$(\beta^2 - \bar{\beta}^2) \int \bar{\psi} \psi \, dA = k^2 \int (n^2 - \bar{n}^2) \bar{\psi} \psi \, dA \tag{24}$$

We now divide Eq. (24) by δT and take the limit $\delta T \rightarrow 0$ to obtain

$$\frac{dn_{\text{eff}}^2}{dT} \int \psi^2 \, dA = \int \frac{dn^2}{dT} \psi^2 \, dA \tag{25}$$

The modal normalisation is

$$\int \psi^2 \, dA = 1 \tag{26}$$

and in each cross sectional region A_i the refractive index n_i is a constant so that Eq. (25) can be expressed as:

$$\frac{dn_{\text{eff}}^2}{dT} = \sum_i \frac{dn_i^2}{dT} \Gamma_i \tag{27}$$

where the power fraction in each region A_i is given by

$$\Gamma_i = \int_{A_i} \psi^2 dA \tag{28}$$

Equation (27) is the generalisation of Eq. (16) to an arbitrary weakly guiding waveguide and is an exact result. It is not the result of a perturbation analysis as ψ is the exact wave function for the entire waveguide cross section and as the temperature changes the wave function can change significantly even though the scalar approximation remains valid. Equation (27) applies not only to fiber based waveguides, but to any weakly guiding structure such as a silica channel waveguide which we discuss in Sect. 6.4. For weak guidance $n_1 \approx n_2$, and for the practical fiber devices which we discuss in the following sections, the temperature controlling regions have the same refractive index n_3 . We can then simplify Eq. (27) to:

$$\frac{dn_{\text{eff}}^2}{dT} = \frac{dn_1^2}{dT} (\Gamma_1 + \Gamma_2) + \frac{dn_3^2}{dT} \Gamma_3 \tag{29}$$

where $\Gamma_3 = \sum \Gamma_i$ and because $\Gamma_1 + \Gamma_2 + \sum \Gamma_i = 1$ we obtain:

$$\frac{dn_{\text{eff}}^2}{dT} = \frac{dn_1^2}{dT} (1 - \Gamma_3) + \frac{dn_3^2}{dT} \Gamma_3 \tag{30}$$

From Eq. (30) the condition for $dn_{\text{neff}}/dT = 0$ is given by:

$$\Gamma_3 = \frac{n_1 \frac{dn_1}{dT}}{n_1 \frac{dn_1}{dT} - n_3 \frac{dn_3}{dT}} \tag{31}$$

Equation (31) has the same form as Eq. (17). It is interesting to note that Eq. (31) contains no details of the fiber construction, and that the value of Γ_3 required for $dn_{\text{eff}}/dT = 0$ can be achieved by many different arrangements of the temperature controlling areas and waveguide geometry. This will become apparent in the examples discussed in the following sections. It is necessary to calculate Γ_3 at only one reference temperature, and is the only parameter that needs to be calculated in order to determine a temperature compensated design. Also, Eq. (31) can be rearranged so that if Γ_3 is known for a particular fiber design then the value of dn_3/dT that is needed for a temperature compensated design can be determined.

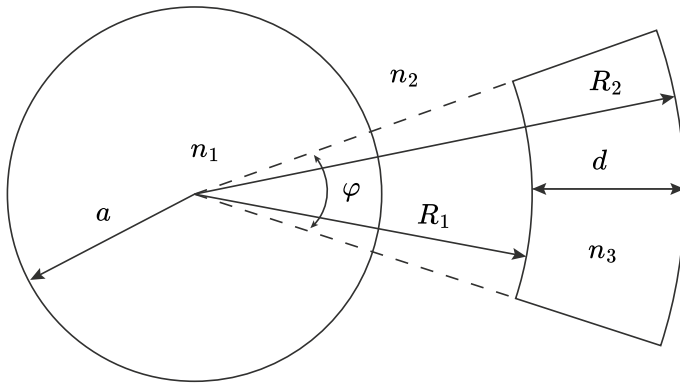


Fig. 4 Geometry of a fiber with an annulus sector used for calculating modal fraction in the temperature controlling region n_3

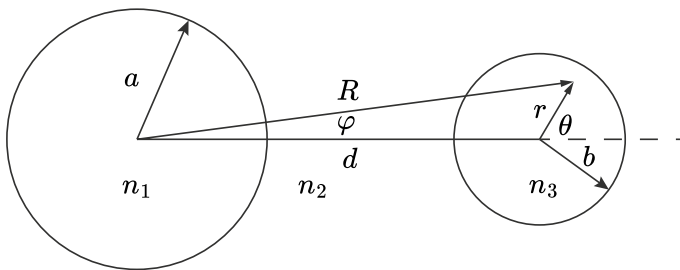


Fig. 5 Geometry of a side hole fiber used for calculating modal fraction in the temperature controlling region n_3

4 Thermal analysis of micro-channel fibers with matched cladding

In this section we consider the case of optical waveguides where the refractive index n_3 of the temperature controlling regions equals that of the cladding index n_2 at a reference temperature T_0 . In this case there is an exact analytical solution for Γ_3 for many waveguides of practical interest and in particular for optical fibers with micro channels which are filled with a temperature controlling fluid or polymer. A wide range of suitable materials are available which can be matched to silica (Cargille; Chemoptics) and we discuss these in detail later in this paper. We consider two fiber geometries of practical interest: the first where the temperature controlling region is formed by the sector of an annulus, Fig. 4, and the second where the temperature control is produced by a side hole channel, Fig. 5.

4.1 Matched cladding annulus sector fiber

The step index fiber analysed in Sect. 2 has limited application. By forming the temperature controlling region from a sector of an annulus surrounding the core a more practical geometry is achieved. This is shown in Fig. 4, where the inner and outer radii of the annulus are R_1 and R_2 respectively, and the annulus sector subtends an angle φ at the center of the fiber core.

Because $n_3 = n_2$ at $T = T_0$, the mode function for $r > a$ is that of a step index fiber described by Eq. (3):

$$\psi = A \frac{J_0(u)}{K_0(w)} \cdot K_0\left(\frac{wr}{a}\right) \text{ for } r > a \tag{32}$$

The modal overlap Γ_3 with the annulus sector is given by:

$$\Gamma_3 = \int_{R_1}^{R_2} \int_0^\varphi \psi^2(r) r dr d\theta \tag{33}$$

The integral in Eq. (33) is easily evaluated using the following result: (Gradshtein and Ryzhik 1980):

$$\int z K_0^2(z) dz = \frac{z^2}{2} [K_0^2(z) - K_1^2(z)] \tag{34}$$

Making use of Eq. (6), we find:

$$\Gamma_3 = \frac{u^2 \varphi}{2\pi V^2 K_1^2(w)} \cdot \left\{ \frac{R_2^2}{a^2} \left[K_0^2\left(\frac{wR_2}{a}\right) - K_1^2\left(\frac{wR_2}{a}\right) \right] - \frac{R_1^2}{a^2} \left[K_0^2\left(\frac{wR_1}{a}\right) - K_1^2\left(\frac{wR_1}{a}\right) \right] \right\} \tag{35}$$

In the limit $\varphi = 2\pi$, $R_1 = a$, and $R_2 = \infty$, Eq. (35) reduces to Eq. (8) as expected.

4.2 Matched cladding side hole fiber

The geometry for a single side hole fiber is shown in Fig. 5 where two cylindrical coordinate systems R, ϕ and r, θ are shown. Because $n_3 = n_2$ at $T = T_0$, the mode function for $R > a$ is again that of a step index fiber described by Eq. (3):

$$\psi = A \frac{J_0(u)}{K_0(w)} \cdot K_0\left(\frac{wR}{a}\right) \text{ for } R > a \tag{36}$$

where R is related to r by $R = \sqrt{r^2 + d^2 + 2rd \cos \theta}$. The modal overlap Γ_3 with the side hole is then given by:

$$\Gamma_3 = \int_0^b \int_0^{2\pi} \psi^2(R) r dr d\theta \tag{37}$$

To calculate the integral in Eq. (37) we use the addition theorem for Bessel functions so that Eq. (37) can be expressed in a single coordinate system (Watson 1995):

$$K_0\left(\frac{wR}{a}\right) = I_0\left(\frac{wr}{a}\right) K_0\left(\frac{wd}{a}\right) + 2 \sum_{p=1}^{\infty} (-1)^p I_p\left(\frac{wr}{a}\right) K_p\left(\frac{wd}{a}\right) \cos(p\theta) \tag{38}$$

Because the $\cos(p\theta)$ terms in Eq. (38) are orthogonal over $\theta = 0$ to 2π , the integral of K_0^2 in Eq. (37) will only involve the sum of squares of the terms in Eq. (38). The integral over r in

Eq. (37) can be calculated with the help of the following formula (Gradshtein and Ryzhik 1980):

$$\int z I_p^2(\lambda z) dz = \frac{z^2}{2} \left\{ I_p^2(\lambda z) - I_{p-1}(\lambda z) I_{p+1}(\lambda z) \right\} \tag{39}$$

Combining Eq. (6) and Eqs. (36) to (39), and after some algebra, the following expression for Γ_3 is obtained:

$$\Gamma_3 = \frac{u^2 b^2}{a^2 V^2 K_1^2(w)} \cdot \left\{ K_0^2(\alpha) \left[I_0^2(\kappa) - I_1^2(\kappa) \right] + 2 \sum_{p=1}^{\infty} K_p^2(\alpha) \left[I_p^2(\kappa) - I_{p-1}(\kappa) I_{p+1}(\kappa) \right] \right\} \tag{40}$$

where $\alpha = wd/a$ and $\kappa = wb/a$. Although Eq. (40) involves an infinite sum over Bessel functions, the series converges rapidly and in practice only a few terms are needed.

4.3 Design of temperature compensated optical fibers with matched cladding side hole fibers

The application of Eq. (35) and Eq. (40) to fiber design is similar and we restrict ourselves to the analysis of side hole fibers based on Eq. (40). Analogous results are obtained using Eq. (35). To illustrate how Eq. (40) can be used to design temperature compensated matched cladding fibers with temperature controlling side hole regions we consider the geometry of Fig. 5 with $a = 4 \mu\text{m}$, $b = 1.5 \mu\text{m}$, $n_1 = 1.451$, $n_2 = 1.445$, $dn_1/dT = dn_2/dT = 8.45 \times 10^{-6}/^\circ\text{C}$ and $dn_3/dT = -389 \times 10^{-6}/^\circ\text{C}$. For a matched cladding fiber, $n_3 = n_2$ at the reference temperature $T_0 = 25^\circ\text{C}$. The refractive index and temperature dependence of n_3 is typical of siloxane and aliphatic / alicyclic hydrocarbon materials readily available from Cargille Laboratories, data sheet: Refractive-Index-Liquid-Series-AA-n-1.4540-at-589.3-nm-and-25°C (Cargille).

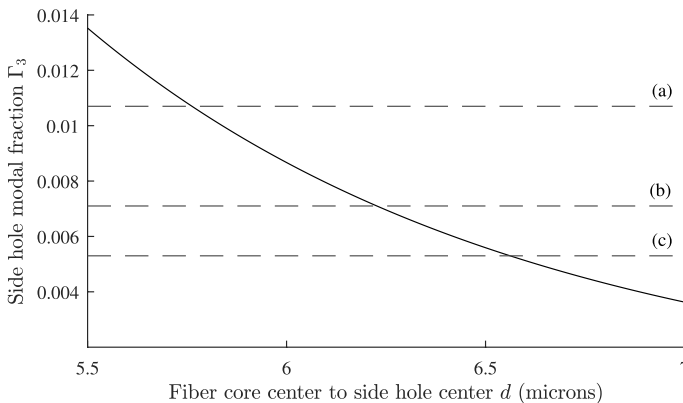


Fig. 6 Plot of Γ_3 as a function of d , separation between core and side hole centers for the geometry in Fig. 5 with matched cladding $n_3 = n_2$ at $T_0 = 25^\circ\text{C}$. The curve was calculated using the analytical result Eq. (40) for a fiber with a single side hole. The horizontal lines show where **a** $\Gamma_3 = 0.0107$, **b** $\Gamma_3 = 0.0071$, and **c** $\Gamma_3 = 0.0053$

Figure 6 shows Γ_3 , calculated using Eq. (40), as a function of d the fiber core center to side hole center. From Eq. (31) the value of Γ_3 for $dn_{\text{eff}}/dT = 0$ is 0.0213. It can be seen in Fig. 6 that there is no value of d that achieves this for a single side hole. Because $n_3 = n_2$ at T_0 , the modal fraction Γ_3 is additive, so that a total $\Gamma_3 = 0.0213$ can be achieved with two side holes, each with $\Gamma_3 = 0.0107$ for $d = 5.76 \mu\text{m}$ and shown by the horizontal line (a). A second design is possible with three side holes each with $\Gamma_3 = 0.0071$, indicated by line (b) for $d = 6.22 \mu\text{m}$. A final design is possible with four side holes each with $\Gamma_3 = 0.0053$, and indicated by line (c) for $d = 6.56 \mu\text{m}$.

We computed the temperature dependence of Δn_{eff} for the four side hole geometry shown in Fig. 7 with the parameters given above, and with $d = 6.56 \mu\text{m}$, and a reference temperature $T_0 = 25^\circ\text{C}$. The results are shown in curve (a) in Fig. 8 and were computed using the finite difference module in FIMMWAVE (Photon Design). Identical results were achieved using the finite element module in FIMMWAVE. Also, shown for comparison in curve (b), is the temperature dependence of Δn_{eff} when $dn/dT = 8.45 \times 10^{-6}/^\circ\text{C}$ for all materials in the waveguide. Increasing the size or number of the sideholes will improve the temperature response. The single graph plotted in Fig. 6 allows all possible temperature compensated designs to be established for the given parameters without the need for repeated numerical calculations of the fiber temperature response.

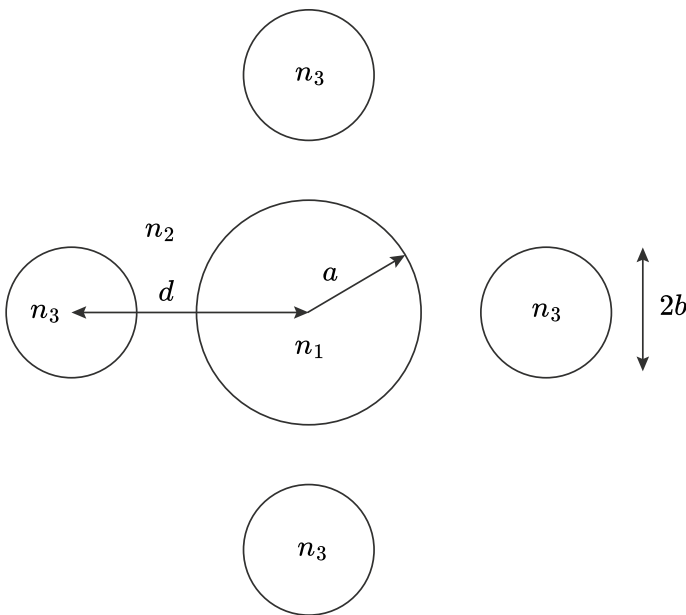


Fig. 7 Geometry of four side hole fiber with side holes arranged symmetrically. The core and cladding have refractive indices n_1 and n_2 respectively, and the temperature controlling regions have the same refractive index n_3

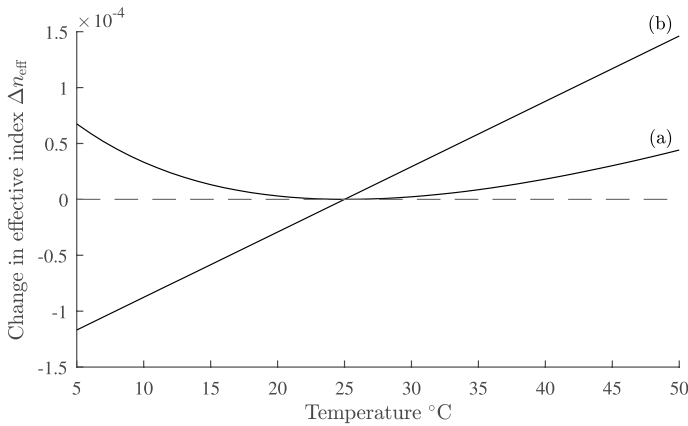


Fig. 8 Plot of fractional change in effective index Δn_{eff} against temperature for a matched cladding four side hole fiber. Curve **a** is for a temperature compensated design with parameters defined in Sect. 4.3, and curve **b** is for an uncompensated fiber where core and cladding both vary as $dn/dT = 8.45 \times 10^{-6}/^{\circ}\text{C}$

5 Thermal analysis of micro-channel fibers with unmatched cladding

When $n_3 \neq n_2$ at T_0 it is no longer possible to calculate Γ_3 analytically for the geometry in Fig. 5. In order to then analyze the four side hole structure in Fig. 7 we must calculate Γ_3 numerically. This was computed using the finite difference module in FIMMWARE (Photon Design) and the following parameters were chosen: $a = 4 \mu\text{m}$, $n_1 = 1.451$, $n_2 = 1.445$, and $n_3 = 1.44$, $dn_1/dT = dn_2/dT = 8.45 \times 10^{-6}/^{\circ}\text{C}$ and $dn_3/dT = -391 \times 10^{-6}/^{\circ}\text{C}$, corresponding to the Cargille refractive index data sheet: Refractive-Index-Liquid-Series-AA-n-1.4500-at-589.3-nm-and-25°C (Cargille). In order to make a direct comparison with the design in the previous section, we set the separation d between the side hole center and core center to $d = 6.56 \mu\text{m}$ and calculate Γ_3 as a function of side hole radius b . From Eq. (31) we require $\Gamma_3 = 0.0213$. Figure 9 shows Γ_3 calculated as a function of b at $T_0 = 25^{\circ}\text{C}$. The horizontal line indicates where $\Gamma_3 = 0.0213$, corresponding to $b = 1.81 \mu\text{m}$. In Fig. 10 curve (a) we plot Δn_{eff} as a function of temperature, and in curve (b) the corresponding result with no temperature compensation. Figure 10 shows an improvement over Fig. 8 of about 15% at $T = 5^{\circ}\text{C}$, reflecting the larger area occupied by the temperature compensating regions.

There have been a number of experimental demonstrations of fibers with microchannels filled with liquids. In one method fibers with microchannels along the length of the fiber have been made using the stack and draw method (Knight et al. 1996). By using capillary action the micro channels can be filled with suitable liquids over lengths of several cms. Using this approach, Huy et al. (2008) and (Naeem and Chung 2014) have demonstrated the temperature control of fiber Bragg gratings written into the core of the fiber. In Huy et al. (2008) fiber Bragg gratings with six and eighteen microchannels were demonstrated with the microchannels filled with liquids provided by Cargille Laboratories (Cargille). In Naeem and Chung (2014) the microchannels were in a photonic crystal fiber and were filled with methanol.

In a second approach the microchannels were formed by laser writing them in the fiber cladding, followed by etching (Song et al. 2025). Access points were provided at the surface of the fiber and the microchannels were liquid filled by capillary action over a

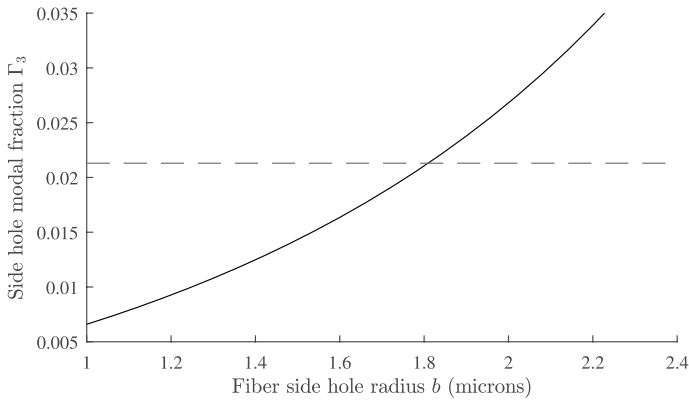


Fig. 9 Plot of Γ_3 as a function of b , the side hole radius for the geometry in Fig. 7 with an unmatched cladding $n_3 \neq n_2$ at $T_0 = 25^\circ\text{C}$. The separation d between the side hole center and fiber core center was set to the value $d = 6.56 \mu\text{m}$ that was calculated in Subsection 4.3. The curve was calculated numerically for a fiber with four side holes. The horizontal lines show where $\Gamma_3 = 0.0213$

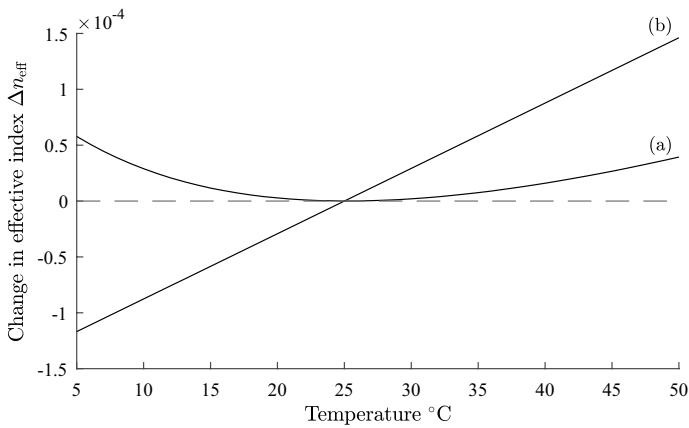


Fig. 10 Plot of fractional change in effective index Δn_{eff} against temperature for an unmatched cladding four side hole fiber. Curve **a** is for a temperature compensated design with parameters defined in Sect. 5, and curve **b** is for an uncompensated fiber where core and cladding both vary as $dn/dT = 8.45 \times 10^{-6}/^\circ\text{C}$

length of 3 mm. In Song et al. (2025) fiber gratings with low temperature sensitivity were demonstrated.

We can estimate the device loss in the same way as in section 2.1. The quoted loss for the liquid in this section is $L = 1.08\text{dB/cm}$ (Cargille). For $\Gamma_3 = 0.0213$ the device loss is then estimated as $\Gamma_3 L = 0.022\text{dB/cm}$ (Adams 1981).

6 Effects of thermal expansion

For a waveguide to be athermal the phase shift of the guided mode should be temperature compensated and this will be affected by thermal expansion. In this section we consider the effects of expansion in both transverse and longitudinal directions. Many optical waveguide devices and components are sensitive to the effects of thermal expansion. Typically, these make use of optical interference or phase change. For example, fiber Bragg gratings are widely used as sensors, including for strain and temperature, or as filters and demultiplexers in communication systems (Kersey et al. 1997). Arrayed waveguide grating demultiplexers based on planar silica-on-silicon technology (Leijtens et al. 2006) are sensitive to expansion of the waveguides, as well as thermal changes to the waveguide refractive indices. We consider the effects of thermal expansion in the transverse direction in Sect. 6.1 and in the longitudinal direction in Sect. 6.2 below.

6.1 Transverse thermal expansion

The largest contribution to transverse thermal expansion will come from the waveguide core as the modal field takes its largest value there. For simplicity we consider a waveguide with a circular core with refractive index n_1 , cladding with index n_2 and temperature controlling regions with refractive indices n_3 equal to n_2 at the reference temperature T_0 . The core radius is a . This means that at temperature T_0 the waveguide mode is that of a step index fiber described by Eqs. (1) to (6). We have shown in Eqs. (25) and (26) that

$$\frac{dn_{\text{eff}}^2}{dT} = \int \frac{dn^2}{dT} \psi^2 dA \tag{41}$$

We now express the radial dependence of n^2 at T_0 as a function of radius r :

$$n^2 = n_1^2 + (n_2^2 - n_1^2) \cdot H(r - a) \tag{42}$$

where H is unit the step function defined by

$$H(x) = \begin{cases} 0 & \text{for } x < 0, \\ 1 & \text{for } x > 0 \end{cases} \tag{43}$$

In Eq. (41) we can write dn^2/dT as:

$$\frac{dn^2}{dT} = \frac{\partial n^2}{\partial T} + \frac{\partial n^2}{\partial r} \cdot \frac{\partial r}{\partial T} \tag{44}$$

The contribution of the term $\partial n^2/\partial T$ in Eq. (44) has been given in Eq. (27), leaving the second term on the right hand side of Eq. (44). Using the properties of the step function this is given by

$$\frac{\partial n^2}{\partial r} \cdot \frac{\partial r}{\partial T} = (n_2^2 - n_1^2) \delta(r - a) \frac{\partial r}{\partial T} \tag{45}$$

The integral in Eq. (41) is straightforward and involves $\psi(a)$, which can be found from Eq. (3). After some further algebra, and making use of Eq. (6), the condition for $dn_{\text{eff}}/dT = 0$ is:

$$\Gamma_3 = \frac{n_1 \frac{dn_1}{dT}}{n_1 \frac{dn_1}{dT} - n_3 \frac{dn_3}{dT}} \times \left\{ 1 + \frac{\alpha(n_1^2 - n_2^2)}{n_1 \frac{dn_1}{dT}} \cdot \frac{u^2}{V^2} \cdot \frac{K_0^2(w)}{K_1^2(w)} \right\} \tag{46}$$

The coefficient of thermal expansion is α , and u , w , and V are defined in Eqs. (1) and (2). The term in braces in Eq. (46) provides a correction to the expression for Γ_3 that was given in Eq. (31). To estimate a typical magnitude of the correction we choose parameters used previously: $\lambda = 1.55 \mu\text{m}$, $a = 4 \mu\text{m}$, $n_1 = 1.451$, $n_2 = 1.445$, $dn_1/dT = 8.45 \times 10^{-6}/^\circ\text{C}$, and $\alpha = 0.55 \times 10^{-6}/^\circ\text{C}$ (Accuratus). From Eqs. (1) to (6) the following values can be determined: $V = 2.1374$, $u/V = 0.7357$, $w = 1.4478$, and $K_0(w)/K_1(w) = 0.7650$. The correction term in Eq. (46) is then:

$$\frac{\alpha(n_1^2 - n_2^2)}{n_1 \frac{dn_1}{dT}} \cdot \frac{u^2}{V^2} \cdot \frac{K_0^2(w)}{K_1^2(w)} = 0.00025 \tag{47}$$

For most applications the correction in Eq. (47) can be neglected. An analysis is possible for a general waveguiding structure, but it is more complex and leads to a similar result.

6.2 Longitudinal thermal expansion

The effects of longitudinal thermal expansion can be expressed in terms of the phase change ϕ along a length L of a waveguide:

$$\phi = n_{\text{eff}}kL \tag{48}$$

where k is the free space wave number. Differentiating Eq. (48) and rearranging we obtain:

$$\frac{1}{\phi} \frac{d\phi}{dT} = \frac{1}{2n_{\text{eff}}^2} \frac{dn_{\text{eff}}^2}{dT} + \alpha \tag{49}$$

Combining Eqs. (49) and (30) the condition for $d\phi/dT = 0$ is:

$$\Gamma_3 = \frac{n_1 \frac{dn_1}{dT}}{n_1 \frac{dn_1}{dT} - n_3 \frac{dn_3}{dT}} \cdot \left\{ 1 + \frac{\alpha n_{\text{eff}}^2}{n_1 \frac{dn_1}{dT}} \right\} \tag{50}$$

Equation (50) is exact within the weakly guiding approximation, and does not rely on perturbation methods. Using the waveguide parameters in the previous section, and noting that $n_1 \geq n_{\text{eff}} \geq n_2$ and $n_1 \approx n_2$ the correction to Γ_3 due to longitudinal expansion can be accurately approximated by

$$\frac{an_{\text{eff}}^2}{n_1 \frac{dn_1}{dT}} \approx an_1 \cdot \frac{1}{\frac{dn_1}{dT}} = 0.094 \tag{51}$$

With this approximation, Eq. (50) is independent of the waveguide geometry and can be written as:

$$\Gamma_3 = \frac{n_1 \frac{dn_1}{dT}}{n_1 \frac{dn_1}{dT} - n_3 \frac{dn_3}{dT}} \cdot \left\{ 1 + an_1 \cdot \frac{1}{\frac{dn_1}{dT}} \right\} \tag{52}$$

Equation (52) represents about a 10% increase in Γ_3 compared to no thermal expansion, and if not compensated will result in a shift of the center wavelength of a fiber Bragg grating or arrayed waveguide grating. We discuss this in the following sections.

6.3 Application to fiber Bragg gratings

For a fiber grating with period Λ , the Bragg wavelength λ_B is given by Kersey et al. (1997):

$$\lambda_B = 2n_{\text{eff}}\Lambda \tag{53}$$

The condition for $d\lambda_B/dT = 0$ is given by Eq. (52) at a reference temperature T_0 . At temperature T the Bragg wavelength is $\lambda_B(T)$, and at temperature T_0 it is $\lambda_B(T_0)$. The shift $\Delta\lambda_B = \lambda_B(T) - \lambda_B(T_0)$ of the Bragg wavelength with temperature is given by:

$$\Delta\lambda_B = \lambda_B(T_0)(\Delta n_{\text{eff}} + \alpha(T - T_0)) \tag{54}$$

where Δn_{eff} was defined in Eq. (18). We consider the geometry of Fig. (7), with $n_3 = n_2$ and $dn_3/dT = -389 \times 10^{-6}/^\circ\text{C}$ at $T_0 = 40^\circ\text{C}$, $b = 1.5 \mu\text{m}$ and the other parameters as given in Sect. 6.1. From Eq. (52) the required value of $\Gamma_3 = 0.0233$. Calculating Eq. (40) and computing a similar graph to Fig. (6), the required separation d between core and side

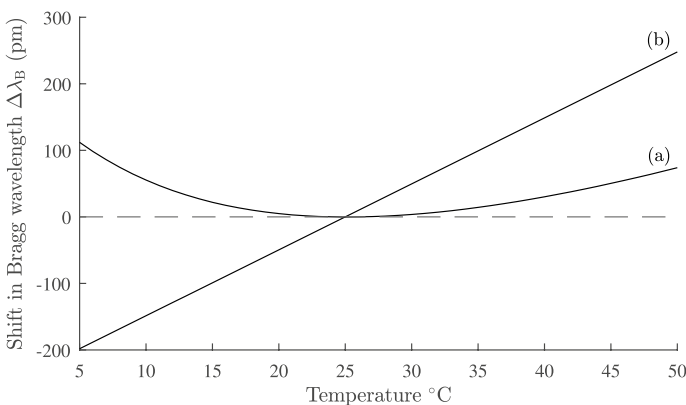


Fig. 11 Shift in picometers of the Bragg wavelength with temperature for a fiber Bragg grating with the fiber geometry in Fig. 7. Curve **a** is for an athermal design, and curve **b** for an uncompensated design. Parameters used are given in Sects. 6.1 and 6.3

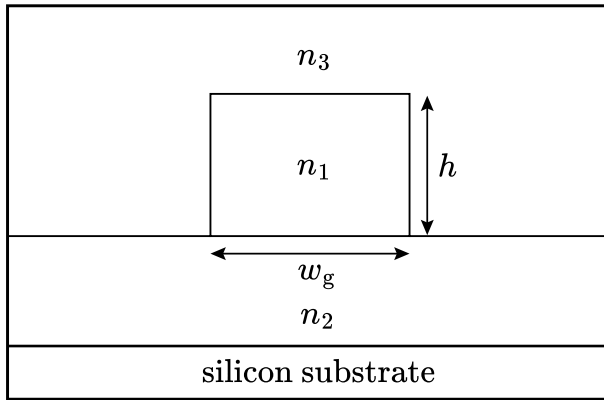


Fig. 12 Cross section of a silica on silicon waveguide. The waveguide materials n_1, n_2 and n_3 are normally silica or germania doped silica, grown on a silicon wafer. An athermal waveguide design results from replacing n_3 with a suitable material with a negative thermal coefficient for the refractive index

hole centers is found to be $d = 6.45 \mu\text{m}$. Using Eq. (54) the change in $\Delta\lambda_B$ with temperature is shown in Fig. 11 curve (a). Also shown for comparison in curve (b) is the change in Bragg wavelength if there is no temperature compensation. The athermal design reduces the maximum shift in $\Delta\lambda_B$ by about 100 pm. Equation (50) allows many other designs to be quickly found without the need to perform multiple finite element simulations of the full temperature response. Equally important, Eq. (50) allows the rapid elimination of unsuccessful designs. It is interesting to note Γ_3 is largest at low temperatures, and falls with increasing temperature, which implies that the grating reflectivity will be slightly reduced at low temperatures.

6.4 Application to silica arrayed waveguide gratings

The arrayed waveguide grating (AWG) is widely used in optical fiber communication systems, with applications including demultiplexing or multiplexing in wavelength division multiplexing (WDM) networks, as well as in other routing devices. A detailed review of AWG technology and design can be found in Leijtens et al. (2006) and (Okamoto 2000). Focusing in an AWG is achieved at a central wavelength λ_c :

$$\lambda_c = \frac{n_{\text{eff}}\Delta L}{m} \tag{55}$$

where ΔL is the length difference between adjacent array waveguides, n_{eff} is the waveguide effective index and m is the diffraction order (Leijtens et al. 2006). The central wavelength, together with the AWG geometry, determines the channel spacing, and free spectral range. A widely used waveguide technology for fabricating AWGs is silica-on-insulator (SOI) (Himeno et al. 1998; Ou 2003). Figure 12 shows the cross section of a typical SOI waveguide grown on a silicon substrate. Normally, the materials n_1, n_2 , and n_3 are silica or germania doped silica, and because of the temperature dependence of n_{eff} , and thermal expansion of ΔL , the central wavelength λ_c varies with temperature so that:

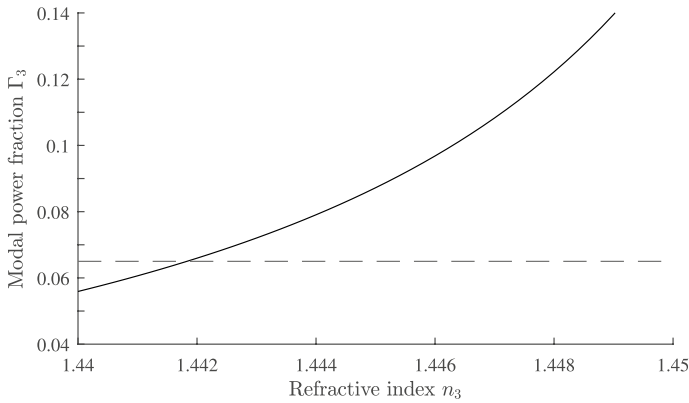


Fig. 13 Plot of Γ_3 as a function of n_3 with $dn_3/dT = -180 \times 10^{-6}/^\circ\text{C}$ for a silica on silicon waveguide with $n_1 = 1.4574$, $n_2 = 1.453$, $dn_1/dT = dn_2/dT = 8.45 \times 10^{-6}/^\circ\text{C}$ and $w_g = h = 8 \mu\text{m}$. The coefficient of thermal expansion of the silicon substrate is $\alpha_{\text{sub}} = 2.63 \times 10^{-6}/^\circ\text{C}$. The horizontal line corresponds to $\Gamma_3 = 0.065$

$$\frac{1}{\lambda_c} \frac{d\lambda_c}{dT} = \frac{1}{2n_{\text{eff}}^2} \frac{dn_{\text{eff}}^2}{dT} + \alpha_{\text{sub}} \tag{56}$$

The coefficient of thermal expansion of the silicon substrate is α_{sub} . In this section we demonstrate how the results derived in this paper can be applied to the design of an athermal AWG by using a polymer for the superstrate material n_3 , Inoue et al. (1997); Li et al. (2007); Wang et al. (2009). Comparing Eqs. (49) and (56) the condition for $d\lambda_c/dT = 0$ is given by Eq. (52) with α replaced by α_{sub} . Referring to Fig. 12 we choose $n_1 = 1.4574$, $n_2 = 1.453$, $dn_1/dT = dn_2/dT = 8.45 \times 10^{-6}/^\circ\text{C}$ and $w_g = h = 8 \mu\text{m}$. This corresponds to a core substrate index difference of 0.3% and t and h chosen so that the modal field matches that of a SMF28 communications fiber (Leijtens et al. 2006). The superstrate n_3 is a

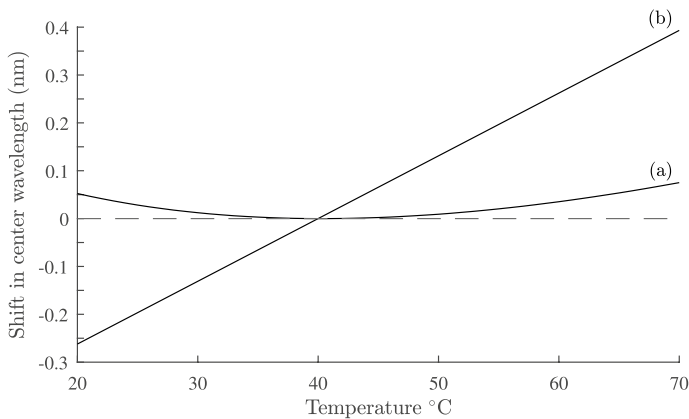


Fig. 14 Shift in nanometers of the center wavelength with temperature for an arrayed waveguide grating based on silica on insulator technology with the parameters described in the text and Fig. 13. Curve **a** is the athermal design, and curve **b** is the response for an uncompensated design

polymer such as ZPU 13-RI with $dn_3/dT = -180 \times 10^{-6}/^\circ\text{C}$ and is available with n_3 in the range 1.43–1.46 from Chemoptics, data sheet: Exguide LFR/ZPU12, 13-RI series (Chemoptics). The coefficient of thermal expansion for silicon is $\alpha_{\text{sub}} = 2.63 \times 10^{-6}/^\circ\text{C}$ (Li et al. 2007; Keil et al. 2001). The reference temperature is set at $T_0 = 40^\circ\text{C}$ and from Eq. (52) the value of Γ_3 so that $d\lambda_c/dT = 0$ is calculated to be $\Gamma_3 = 0.065$. Figure 13 shows part of a plot of Γ_3 computed as a function of n_3 , from which we find $n_3 = 1.442$ for $\Gamma_3 = 0.065$. The shift $\Delta\lambda_c = \lambda_c(T) - \lambda_c(T_0)$ of the center wavelength is:

$$\Delta\lambda_c = \lambda_c(T_0)(\Delta n_{\text{eff}} + \alpha_{\text{sub}}(T - T_0)) \tag{57}$$

This is plotted in Fig. 14, curve (a) as a function of temperature over the range $T = 20$ to 70°C . With temperature compensation the shift in λ_c is about 0.05 nm. For comparison in curve (b), there is a shift of more than 0.6 nm in λ_c across the same temperature range when there is no temperature compensation. A similar result, computed by a different approach, was reported in Inoue et al. (1997); Li et al. (2007).

The loss of the polymer ZPU 13-RI is quoted as $L = 0.31\text{dB/cm}$ (Chemoptics), and with $\Gamma_3 = 0.065$ corresponds to a device loss of $\Gamma_3 L = 0.02\text{dB/cm}$.

7 Analysis of strongly guiding waveguides with vector modes

The analysis presented so far applies to weakly guiding waveguides where there is a small difference between refractive indices. The modal fields are accurately described by a scalar wave function and wave equation. For strongly guiding waveguides where the refractive index differences are large, such as silicon-on-insulator (Jalali et al. 1998), the modes must be described by fully vector electric and magnetic fields and Eq. (27) will no longer apply. In this section we derive an expression for dn_{eff}/dT that is valid for a fully vector theory. It is straightforward to extend the analysis that follows to a general anisotropic waveguide.

We assume a time dependence $\exp(i\omega t)$ for the fields and Maxwell’s equations are given by:

$$\nabla \times \mathbf{E} = -i\omega\mu_0\mathbf{H} \tag{58}$$

$$\nabla \times \mathbf{H} = i\omega\varepsilon_0 n^2 \mathbf{E} \tag{59}$$

The electric and magnetic fields at temperature T are \mathbf{E} and \mathbf{H} , and at temperature $\bar{T} = T + \delta T$ they are $\bar{\mathbf{E}}$ and $\bar{\mathbf{H}}$. We introduce the vector \mathbf{F} defined by Snyder and Love (1984):

$$\mathbf{F} = \mathbf{E} \times \bar{\mathbf{H}}^* + \bar{\mathbf{E}}^* \times \mathbf{H} \tag{60}$$

Using the two-dimensional form of the divergence theorem, the following relation holds:

$$\int_A \nabla \cdot \mathbf{F} dA = \frac{\partial}{\partial z} \int_A \mathbf{F} \cdot \hat{\mathbf{z}} dA + \oint \mathbf{F} \cdot \hat{\mathbf{n}} dl \tag{61}$$

where A is the waveguide cross section, $\hat{\mathbf{z}}$ is the unit vector along the waveguide, and the line integral is around the boundary of A with $\hat{\mathbf{n}}$ the outward normal unit vector on l . If we let the cross section A be the infinite cross section A_∞ , and assume that the fields vanish on the boundary, then the line integral vanishes and Eq. (61) becomes

$$\int_{A_\infty} \nabla \cdot \mathbf{F} \, dA = \frac{\partial}{\partial z} \int_{A_\infty} \mathbf{F} \cdot \hat{\mathbf{z}} \, dA \tag{62}$$

The electric and magnetic fields can be written in terms of the waveguide modal fields \mathbf{e} and \mathbf{h} at temperature T as:

$$\mathbf{E} = \mathbf{e} \exp(-i\beta z) \tag{63}$$

$$\mathbf{H} = \mathbf{h} \exp(-i\beta z) \tag{64}$$

and at temperature $\bar{T} = T + \delta T$ as:

$$\bar{\mathbf{E}} = \bar{\mathbf{e}} \exp(-i\bar{\beta}z) \tag{65}$$

$$\bar{\mathbf{H}} = \bar{\mathbf{h}} \exp(-i\bar{\beta}z) \tag{66}$$

where $\bar{\beta} = \beta(T + \delta T)$. The modal fields \mathbf{e} and \mathbf{h} are normalised so that:

$$\int_{A_\infty} \mathbf{e} \times \mathbf{h}^* \cdot \hat{\mathbf{z}} \, dA = \int_{A_\infty} \mathbf{e}^* \times \mathbf{h} \cdot \hat{\mathbf{z}} \, dA = 1 \tag{67}$$

We evaluate the integrands on each side of Eq. (62). Taking the divergence of Eq. (60) we have:

$$\nabla \cdot \mathbf{F} = \bar{\mathbf{H}}^* \cdot \nabla \times \mathbf{E} - \mathbf{E} \cdot \nabla \times \bar{\mathbf{H}}^* + \mathbf{H} \cdot \nabla \times \bar{\mathbf{E}}^* - \bar{\mathbf{E}}^* \cdot \nabla \times \mathbf{H} \tag{68}$$

Using Eqs. (58), (59) and Eqs. (63) to (66) we can simplify Eq. (62):

$$\nabla \cdot \mathbf{F} = i\omega\epsilon_0(n^2 - \bar{n}^2)\mathbf{e} \cdot \bar{\mathbf{e}}^* \exp(i(\bar{\beta} - \beta)z) \tag{69}$$

where $\bar{n} = n(T + \delta T)$. Using Eqs. (63) to (66) we find:

$$\frac{\partial \mathbf{F}}{\partial z} = (i(\bar{\beta} - \beta))(\mathbf{e} \times \bar{\mathbf{h}}^* + \bar{\mathbf{e}}^* \times \mathbf{h}) \exp(i(\bar{\beta} - \beta)z) \tag{70}$$

Combining Eqs. (62), (69) and (70), together with the normalisation condition Eq. (67), and taking the limit $\delta T \rightarrow 0$ so that $\bar{\mathbf{e}} \rightarrow \mathbf{e}$ and $\bar{\mathbf{h}} \rightarrow \mathbf{h}$ we find:

$$\frac{dn_{\text{eff}}}{dT} = \frac{1}{2} \sqrt{\frac{\epsilon_0}{\mu_0}} \int_{A_\infty} \frac{dn^2}{dT} |\mathbf{e}|^2 \, dA \tag{71}$$

If $n = n_i$ in each region A_i of the waveguide, we can rewrite Eq. (71) as follows:

$$\frac{dn_{\text{eff}}}{dT} = \frac{1}{2} \sqrt{\frac{\epsilon_0}{\mu_0}} \sum_i \frac{dn_i^2}{dT} \int_{A_i} |\mathbf{e}|^2 \, dA \tag{72}$$

The extension of this analysis to anisotropic fibers is straightforward and in place of Eq. (71) we find:

$$\frac{dn_{\text{eff}}}{dT} = \frac{1}{2} \sqrt{\frac{\epsilon_0}{\mu_0}} \int_{A_\infty} e_k \frac{dn_{kl}^2}{dT} e_l^* \, dA \tag{73}$$

The refractive index tensor n_{kl}^2 is related to the dielectric tensor ϵ_{kl} by $n_{kl}^2 = \epsilon_{kl}$, and summation over the repeated indices k and l is implied in Eq. (73).

Equation (72) is exact and should be compared to the weakly guiding result Eq. (27). An important difference is that in general, the integral in Eq. (72) is not the fraction of modal power in the cross section A_i , which means that Eq. (27) should not be applied to a strongly guiding waveguide such as silicon on insulator (Jalali et al. 1998). An exception is the TE mode on a planar optical waveguide when it is straightforward to show that Eq. (72) is the same as Eq. (27).

We shall now show transverse thermal expansion of a strongly guiding waveguide is no longer negligible, as was demonstrated in Sect. 6.1 for the case of weak guidance. If we repeat the analysis of Sect. 6.1 and use Eqs. (41) to (45) in Eq. (71), we can estimate the contribution of transverse thermal expansion of the waveguide core to dn_{eff}/dT from Eq. (71) as:

$$\pi\alpha^2 \sqrt{\frac{\epsilon_0}{\mu_0}} \alpha(n_1^2 - n_2^2) | \mathbf{e}(a) |^2 \tag{74}$$

For a silicon waveguide, the coefficient of thermal expansion $\alpha = 2.63 \times 10^{-6}/^\circ\text{C}$, and $(n_1^2 - n_2^2) \approx 10$, compared to the values for silica used in Sect. 6.1 of $\alpha = 0.55 \times 10^{-6}/^\circ\text{C}$ and $(n_1^2 - n_2^2) = 0.017$. This is a ratio of about 2780 which implies that transverse thermal expansion effects are expected to be significant for strongly guiding structures.

Finally, we show that Eq. (72) reduces to Eq. (27) in the weak guidance limit. In a weakly guiding waveguide \mathbf{e} and \mathbf{h} are orthogonal and transverse to the z direction, so that they can be written as:

$$\mathbf{e} = \hat{\mathbf{x}} e_x \exp(-i\beta z) \tag{75}$$

$$\mathbf{h} = \hat{\mathbf{y}} h_y \exp(-i\beta z) \tag{76}$$

where $\hat{\mathbf{x}}$ and $\hat{\mathbf{y}}$ are unit vectors along the x and y axes. The normalization condition Eq. (67) is then:

$$\int_{A_\infty} e_x h_y^* dA = 1 \tag{77}$$

Taking the y -component of Eq. (58) we find that e_x can be expressed in terms of h_y as:

$$e_x = \frac{1}{n_{\text{eff}}} \sqrt{\frac{\mu_0}{\epsilon_0}} h_y \tag{78}$$

Then we can write $| \mathbf{e} |^2$ as:

$$| \mathbf{e} |^2 = \frac{1}{n_{\text{eff}}} \sqrt{\frac{\mu_0}{\epsilon_0}} e_x h_y^* \tag{79}$$

Equation (72) then becomes

$$\frac{dn_{\text{eff}}}{dT} = \frac{1}{2n_{\text{eff}}} \sum_i \frac{dn_i^2}{dT} \int_{A_i} e_x h_y^* dA \tag{80}$$

Because of the normalization condition Eq. (77), the integral in Eq. (80) is Γ_i , the fraction of modal power in the cross section A_i , which finally gives us

$$\frac{dn_{\text{eff}}^2}{dT} = \sum_i \frac{dn_i^2}{dT} \Gamma_i \quad (81)$$

This is the same as the scalar result Eq. (27).

8 Conclusion

In this paper we have presented an exact analysis of the temperature dependence of optical waveguides with thermo-optic controlling regions, either as micro channels around a fiber core, or as cladding regions in a planar waveguide structure. We have shown that the condition for zero rate of change with temperature of the waveguide effective index is determined by a simple but exact equation that relates the temperature variation of the effective index to the fractions of modal field in the different waveguide regions. This condition is independent of the waveguide structure and provides a unified approach for determining temperature compensated designs, or waveguide structures for which no such design is possible.

Our analysis requires the computation of a single parameter at one temperature: the modal power fraction in the temperature compensating regions. Some waveguides of practical interest have exact solutions, as described in Sects. 2 and 4, and in these cases a complete analytical solution is possible for a temperature compensated waveguide design. For those waveguides for which no analytical solution exists we have calculated the modal power fraction using finite difference or finite element methods, such as FIMMWAVE (Photon Design). Again, only one parameter at a single temperature needs to be calculated. This can be contrasted with analyses using finite element methods where the waveguide behavior must be repeatedly calculated over a range of temperatures (Gyflason et al. 2012; Man et al. 2019; Mothe et al. 2008; Wang et al. 2009).

We have shown how the effects of thermal expansion can be included in order to produce athermal designs. We applied our analysis to a variety of optical waveguiding structures and devices but without attempting to produce optimised designs.

We extended the analysis to strongly guiding waveguides where the modal field must be described by a full vector equation. The condition for $dn_{\text{eff}}/dT = 0$ can no longer be written in terms of the fractions of modal power in each refractive index region, and Eq. (27) should not be used for strongly guiding waveguides. The effects of transverse thermal expansion can no longer be ignored. Finally, we demonstrated that the vector result reduces to the scalar result Eq. (27) in the weak guidance limit.

Authors contribution All authors contributed to the analysis in this article. All authors read and approved the final manuscript.

Funding Mohan Wang, and Julian A. J. Fells were supported by the Engineering and Physical Sciences Research Council (EP/T00326X/1).

Data availability No datasets were generated or analysed during the current study.

Declarations

Conflict of interest The authors have no relevant financial or non-financial interests to disclose.

Consent for publication All authors have consented to the publication of this article.

Open Access This article is licensed under a Creative Commons Attribution 4.0 International License, which permits use, sharing, adaptation, distribution and reproduction in any medium or format, as long as you give appropriate credit to the original author(s) and the source, provide a link to the Creative Commons licence, and indicate if changes were made. The images or other third party material in this article are included in the article's Creative Commons licence, unless indicated otherwise in a credit line to the material. If material is not included in the article's Creative Commons licence and your intended use is not permitted by statutory regulation or exceeds the permitted use, you will need to obtain permission directly from the copyright holder. To view a copy of this licence, visit <http://creativecommons.org/licenses/by/4.0/>.

References

- Abramowitz, M., Stegun, I.A. (eds.): Handbook of Mathematical Functions. Dover Publ, New York (2013)
- Accurat: Accurat ceramic corporation, Phillipsburg, New Jersey 08865, USA, (2025) <https://www.accuratus.com/>
- Adams, M.J.: An Introduction to Optical Waveguides. Wiley, Chichester (1981)
- Arfken, G.B., Weber, H.J., Harris, F.E.: Mathematical Methods for Physicists: A Comprehensive Guide, 7th, ed Elsevier, Amsterdam (2013)
- Ascorbe, J., Corres, J.M., Matias, I.R., Arregui, F.J.: High sensitivity humidity sensor based on cladding-etched optical fiber and lossy mode resonances. *Sens. Actuators B: Chem.* **233**, 7–16 (2016)
- Cargille: Cargille laboratories, NJ 07009 USA, (2025) <https://www.cargille.com/>
- Chemoptics: Chemoptics, 261 Techno-2-ro, Yuseong-gu, Daejeon, Republic of Korea, (2025) <https://www.chemoptics.co.kr/en/>
- Fokoua, E.N., Petrovich, M.N., Bradley, T., Poletti, F., Richardson, D.J., Slavík, R.: How to make the propagation time through an optical fiber fully insensitive to temperature variations. *Optica* **4**(6), 659–668 (2017)
- Gao, S., Jin, L., Ran, Y., Sun, L.-P., Li, J., Guan, B.-O.: Temperature compensated microfiber Bragg gratings. *Optics Express* **20**(16), 18281–18286 (2012)
- Gradshteyn, I.S., Ryzhik, I.S.: Table of Integrals, Series, and Products, 2nd, edition Academic Press, London (1980)
- Gyllfason, K.B., Romero, A.M., Sohlström, H.: Reducing the temperature sensitivity of SOI waveguide-based biosensors. In: Silicon Photonics and Photonic Integrated Circuits III, vol. 8431, pp. 68–82. SPIE, Brussels, Belgium (2012)
- Hale, Z.M., Payne, F.P.: Fluorescent sensors based on tapered single-mode optical fibres. *Sens. Actuators B: Chem.* **17**(3), 233–240 (1994)
- Hale, Z.M., Payne, F.P., Marks, R.S., Lowe, C.R., Levine, M.M.: The single mode tapered optical fibre loop immunosensor. *Biosens. Bioelectron.* **11**(1), 137–148 (1996)
- Henry, W.M., Payne, F.P.: Solid-state tapered optical fibre devices. *Optical Quant. Electron.* **27**(3), 185–191 (1995)
- Himeno, A., Kato, K., Miya, T.: Silica-based planar lightwave circuits. *IEEE J. Select. Top. Quant. Electron.* **4**(6), 913–924 (1998)
- Huy, M.C.P., Laffont, G., Dewynter, V., Ferdinand, P., Pagnoux, D., Dussardier, B., Blanc, W.: Passive temperature-compensating technique for microstructured fiber Bragg gratings. *IEEE Sens. J.* **8**(7), 1073–1078 (2008)
- Inoue, Y., Kaneko, A., Hanaw, F., Takahashi, H., Hattori, K., Sumida, S.: Athermal silica-based arrayed-waveguide grating (AWG) multiplexer. In: Integrated Optics and Optical Fibre Communications, 11th International Conference On, and 23rd European Conference on Optical Communications (Conf. Publ. No.: 448), vol. 5, pp. 33–365 (1997)
- Jalali, B., Yegnanarayanan, S., Yoon, T., Yoshimoto, T., Rendina, I., Coppinger, F.: Advances in silicon-on-insulator optoelectronics. *IEEE J. Select. Top. Quant. Electron.* **4**(6), 938–947 (1998)
- Kamei, S., Inoue, Y., Shibata, T., Kaneko, A.: Low-loss and compact silica-based athermal arrayed waveguide grating using resin-filled groove. *J. Lightw. Technol.* **27**(17), 3790–3799 (2009)
- Keil, N., Yao, H.H., Zawadzki, C.: Athermal polarisation-independent arrayed-waveguide grating (AWG) multiplexer using an all-polymer approach. *Appl. Phys. B* **73**(5), 619–622 (2001)

- Kersey, A.D., Davis, M.A., Patrick, H.J., LeBlanc, M., Koo, K.P., Askins, C.G., Putnam, M.A., Friebele, E.J.: Fiber grating sensors. *J. Lightw. Technol.* **15**(8), 1442–1463 (1997)
- Kim, K.T., Kim, I.S., Lee, C.-H., Lee, J.: A temperature-insensitive cladding-etched fiber Bragg grating using a liquid mixture with a negative thermo-optic coefficient. *Sensors* **12**(6), 7886–7892 (2012)
- Knight, J.C., Birks, T.A., Russell, P.S.J., Atkin, D.M.: All-silica single-mode optical fiber with photonic crystal cladding. *Optics Lett.* **21**(19), 1547–1549 (1996)
- Leijtens, X.J.M., Kuhlouw, B., Smit, M.K.: Arrayed Waveguide Gratings. In: Venghaus, H. (ed.) *Wavelength Filters in Fibre Optics*, pp. 125–187. Springer, Berlin (2006)
- Leviton, D.B., Frey, B.J.: Temperature-dependent absolute refractive index measurements of synthetic fused silica. In: *Optomechanical Technologies for Astronomy*, vol. 6273, pp. 800–810. International Society for Optics and Photonics, Orlando, Florida (2006)
- Li, D.-L., Ma, C.-S., Qin, Z.-K., Zhang, H.-M., Zhang, D.-M., Liu, S.-Y.: Design of athermal arrayed waveguide grating using silica/polymer hybrid materials. *Optica Appl.* **37**(3), 305–312 (2007)
- Man, W., Zhang, C., Huang, J., He, Q.: Optimization design of temperature-insensitive Bragg gratings inscribed in ethanol-filled photonic crystal fibers. *Optical Eng.* **58**(11), 116101 (2019)
- Meunier, D., Schruyvers, J., Gonzales Palla, R., Mendoza, C., Calberg, C., Heinrichs, B., Pirard, S., Mahy, J.G.: Controlled-chemical etching of the cladding in optical fibers for the design of analytical sensors. *Optical Fiber Technol.* **78**, 103328 (2023)
- Mothe, N., Pagnoux, D., Huy, M.C.P., Dewinter, V., Laffont, G., Ferdinand, P.: Thermal wavelength stabilization of Bragg gratings photowritten in hole-filled microstructured optical fibers. *Optics Express* **16**(23), 19018–19033 (2008)
- Naeem, K., Chung, Y.: Strain and temperature discrimination using PCF Bragg-gratings filled with different liquids. In: 2014 OptoElectronics and Communication Conference and Australian Conference on Optical Fibre Technology, pp. 795–796 (2014)
- Okamoto, K.: *Fundamental Optical Waveguides*. Academic Press, San Diego (2000)
- Ou, H.: Different index contrast silica-on-silicon waveguides by PECVD. *Electron. Lett.* **39**(2), 212–213 (2003)
- Pendock, G.J., MacKenzie, H.S., Payne, F.P.: Dye lasers using tapered optical fibers. *Appl. Optics* **32**(27), 5236–5242 (1993)
- Photon design: Photon design, Oxford, OX4 1TW United Kingdom, url = <http://www.photond.com/index.htm>
- Snyder, A.W., Love, J.D.: *Optical Waveguide Theory*. Springer, Boston (1984)
- Song, Z., Wang, M., Payne, F.P., Salter, P.S., Liu, T., Elston, S.J., Booth, M.J., Morris, S.M., Fells, J.A.J.: Fiber Bragg gratings with micro-engineered temperature coefficients. *Adv. Optical Mater.* (2025). <https://doi.org/10.1002/adom.202402726>
- Wang, X., Xiao, S., Zheng, W., Wang, F., Li, Y., Hao, Y., Jiang, X., Wang, M., Yang, J.: Athermal silicon arrayed waveguide grating with polymer-filled slot structure. *Optics Commun.* **282**(14), 2841–2844 (2009)
- Wang, L., Bogaerts, W., Dumon, P., Selvaraja, S.K., Teng, J., Pathak, S., Han, X., Wang, J., Jian, X., Zhao, M., Baets, R., Morthier, G.: Athermal arrayed waveguide gratings in silicon-on-insulator by overlaying a polymer cladding on narrowed arrayed waveguides. *Appl. Optics* **51**(9), 1251–1256 (2012)
- Watson, G.N.: *A Treatise on the Theory of Bessel Functions*. Cambridge University Press, Cambridge (1995)
- Ye, W.N., Michel, J., Kimerling, L.C.: Athermal high-index-contrast waveguide design. *IEEE Photon. Technol. Lett.* **20**(11), 885–887 (2008)
- Zaca-Morán, P., Padilla-Martínez, J.P., Pérez-Corte, J.M., Dávila-Pintle, J.A., Ortega-Mendoza, J.G., Morales, N.: Etched optical fiber for measuring concentration and refractive index of sucrose solutions by evanescent waves. *Laser Phys.* **28**(11), 116002 (2018)